LIMNOLOGY and OCEANOGRAPHY

ASLO

Limnol. Oceanogr. 9999, 2020, 1–19

doi: 10.1002/lno.11394

Hydrologic controls on CO_2 chemistry and flux in subtropical lagoonal estuaries of the northwestern Gulf of Mexico

Hongming Yao ,* **Melissa R. McCutcheon** , **Cory J. Staryk, Xinping Hu**
Department of Physical and Environmental Science, Texas A&M University-Corpus Christi, Corpus Christi, Texas

Abstract

Estuaries are generally considered a source of CO_2 to the atmosphere, although with significant uncertainties in magnitude and controlling factors between and within estuaries. We studied four northwestern Gulf of Mexico estuaries that experience extreme hydrologic conditions between April 2014 and February 2017 to determine the role of dry/wet cycle on estuarine CO_2 system. Annual air–water CO_2 flux ranged from 2.7 to 35.9 mol·C·m^{-2}·yr^{-1}; CO_2 flux declined by approximately an order of magnitude along with declining river discharge. Episodic flooding made CO_2 flux differ between dry (–0.7 to 20.9 mmol·C·m^{-2}·d^{-1}) and wet (11.6–170.0 mmol·C·m^{-2}·d^{-1}) conditions. During wet condition, increases in dissolved inorganic carbon (DIC) and total alkalinity (TA) significantly elevated CO_2 degassing. Furthermore, ventilation of river-borne CO_2 strengthened degassing when estuaries became overwhelmingly river-dominated. During flood relaxation, all estuaries experienced heightened productivity, evidenced by DIC and TA consumption in the mid-salinity range (10–30). When prolonged drought led to hypersalinity (>36.5), biogeochemical and evaporative effects enhanced DIC and TA consumption and CO_2 degassing. Due to flooding and high wind speeds, these estuaries were a strong CO_2 source during spring and summer. Then they transitioned to a weak CO_2 source or sink during the fall. Low temperatures further depressed CO_2 efflux during winter except when a pulse of freshwater input occurred. This study demonstrates that changes in the hydrologic condition of estuaries, such as dry/wet cycle and river discharge gradient, will greatly alter air–water CO_2 flux and estuarine contribution to the global carbon budget.

In the highly dynamic transition zone where the land meets the ocean, estuaries are generally net heterotrophic and therefore act as a CO_2 source to the atmosphere with substantial spatiotemporal variations in CO_2 flux (Laruelle et al. 2010; Chen et al. 2013). Coastal lagoons, a major type of estuary, are typically shallow (< 5 m) and have limited exchange with the adjacent ocean (Boynton et al. 1996). The estimated CO_2 flux (17.3 ± 16.6 mol·C·yr^{-1}·m^{-2}) from coastal lagoons is almost the same as that from fjords (17.5 ± 14.0 mol·C·yr^{-1}·m^{-2}), the world's largest estuarine type; together lagoons and fjords account for two-thirds of the total global estuarine area (the former accounts for 23.6% and the later accounts for 42.7%; Laruelle et al. 2010; Bauer et al. 2013). North America has 34% of the world's lagoons (Cromwell 1971), most of which are located in the Gulf of Mexico (GOM; Dürr et al. 2011). Yao and Hu (2017) suggested that Mission-Aransas Estuary in the northwestern GOM (nwGOM) is a CO_2 source with an estimated CO_2 flux at 12.3 ± 3.3 mol·C·m^{-2}·yr^{-1}. The lack of data for the rest of the nwGOM region makes it difficult to accurately quantify regional estuarine CO_2 flux, especially since the region is subject to a strong latitudinal climatic gradient.

There are seven major estuaries along the 600 km of Texas coastline in the nwGOM (Longley 1994). In each of these estuaries, there is a secondary bay (or upper estuary in this study) that directly receives freshwater inflow from at least one major river and a larger primary bay (or lower estuary in this study) that has restricted connection to the nwGOM due to the barrier island chain. Despite the similar geomorphic structure and physiography, these estuaries are remarkably hydrologically diverse due to the presence of a climatic gradient (Montagna et al. 2012). This gradient (wetter in northeast and drier in southwest) causes a difference in freshwater balance of almost two orders of magnitude, decreasing from northeast to southwest (Longley 1994; Montagna et al. 2012). Both recorded data (Texas Water Development Board, http://www.twdb.texas.gov) and a climate projection (Milliman et al. 2008) indicate that these estuaries are subject to prolonged periods of drought punctuated by periods of intense flooding, resulting in extreme changes in hydrologic conditions in relatively short periods of

*Correspondence: hyao1@islander.tamucc.edu

time (weeks to months). The fast and intense hydrologic transitions make the nwGOM coast an ideal place to study hydrologic influence on estuarine CO_2 chemistry and flux.

To better understand the role of subtropical lagoons in regional and global air–water CO_2 flux budgets and to investigate the influence of the dry–wet cycle on the estuarine carbonate system under the context of global climate change, we characterized CO_2 chemistry and flux based on a 3-yr data set (2014–2017) in four estuaries. We examined spatial and temporal variations in CO_2 flux and identified the primary controls on both carbonate chemistry and CO_2 flux.

Methods

Study sites

Four nwGOM estuaries (Fig. 1)—Lavaca-Colorado Estuary (LCE), Guadalupe Estuary (GE), Mission-Aransas Estuary (MAE), and Nueces Estuary (NE)—were sampled between April 2014 and February 2017. These shallow estuaries (1–5 m in depth) are located in the middle of the nwGOM coast along a freshwater inflow gradient (Russell and Montagna 2007). We sampled LCE, GE, and NE seasonally in April, July, October, and January of each year from 2014 to 2017 (with the exception of 2017, when we sampled in February instead of January). These sampling months represent spring, summer, fall, and winter, respectively. Sampling occurred more frequently (biweekly to monthly) in MAE (Yao and Hu 2017). River samples were collected every other month between October 2015 and June 2017, with additional field campaigns immediately following flooding events. Carbonate chemistry of river end-members for these estuaries were then derived from the averages of corresponding riverine data. Ocean end-member was studied for all four estuaries, and its dissolved inorganic carbon (DIC) and pCO_2 were calculated using pH and total alkalinity (TA) from Texas Commission on Environmental Quality (https://www.tceq.texas.gov/) quarterly field campaigns.

Our sampling stations spanned from the river mouth(s) to tidal inlet in each estuary. Samples were taken from the surface and bottom of the water column in the estuaries (and from the surface only in the rivers) using a Van Dorn water sampler. Samples were preserved following the standard protocol for ocean CO_2 studies (Dickson et al. 2007). All field sampling occurred during the daytime. In-situ data (temperature, pressure, and dissolved oxygen [DO]) were obtained using a calibrated YSI 6600 V2 data sonde.

Monthly river discharge data were obtained from the U.S. Geological Survey (USGS) real-time streamflow record (http://waterdata.usgs.gov/tx/nwis/rt). Hourly wind speed and barometric pressure data were obtained from National Oceanic and Atmospheric Administration's (NOAA) weather stations along the coast (https://tidesandcurrents.noaa.gov/stations.html). Daily mean wind speed and barometric pressure were calculated for the sampling days. Wind speeds from anemometers that were typically installed at $\sim$ 3 m height above water were converted to wind speeds at 10 m height using the wind profile power law (Hsu et al. 1994).

Chemical analyses

Water samples were analyzed for carbonate system parameters—TA, DIC, and pH. Briefly, DIC and TA were both analyzed at 22 ± 0.1°C. DIC was determined by acidifying 0.5 mL of sample with 10% phosphoric acid and quantifying the extracted CO_2 on an AS-C3 DIC analyzer (Apollo SciTech). TA was determined using the Gran Titration (Gran 1952) on an AS-ALK2 alkalinity titrator (Apollo SciTech). Both DIC and TA analyses had a precision of $\pm$ 0.1%. Certified reference material (CRM Batch#142, 156, 159; Dickson et al. 2003) was used throughout our analyses for data quality control and assurance.

pH was measured using either a spectrophotometric method (when salinity > 20, measured at 25 ± 0.1°C, Carter et al. 2013) or an Orion™ Ross pH electrode (when salinity < 20, measured at 25 ± 0.1°C, calibrated with National Bureau of Standards (NBS) buffers at 4.01, 7.00, and 10.01). pH measurements had a precision of $\pm$ 0.004 for the spectrophotometric method and $\pm$ 0.01 for the electrode. All potentiometric pH values from the electrode were converted from the NBS scale to the total scale. Salinity was measured using a benchtop salinometer calibrated with MilliQ water and a known-salinity CRM.

The partial pressure of CO_2 in the water ($pCO_{2,water}$) and pH at in-situ temperature were calculated in the CO2SYS program (Lewis and Wallace 1998) using DIC and lab-measured pH at 25°C. We chose DIC and pH as the input variables to avoid possible errors associated with noncarbonate alkalinity when TA is used in speciation calculations (Abril 2015). Carbonic acid dissociation constants (K_1, K_2) from Millero (2010) and the bisulfate dissociation constant from Dickson (1990) were used. In our previous study (Yao and Hu 2017), a salinity-dependent ΔTA (i.e., $TA_{measured} - TA_{calculated}$) was observed. Orr et al. (2018) suggested 2.6–3.2% uncertainty in pCO_2 when pairing DIC and pH for calculations in CO2SYS, which equated to approximately an error of 8–16 μatm in calculated pCO_2 in this study (based on the annual average pCO_2). In addition, our calculated $pCO_{2,water}$ matched well ($\pm$ 20 μatm) with real-time monitoring values using a calibrated SAMICO_2 sensor (McCutcheon et al. unpubl.).

Air–water CO_2 flux calculation

We used Eq. 1 to calculate the air–water CO_2 flux:

$$F = k \cdot K_0 (pCO_{2,water} - pCO_{2,air}), \quad (1)$$

where k ($m \cdot d^{-1}$) is the gas transfer velocity as a function of wind speed, K_0 ($mol \cdot m^{-3} \cdot atm^{-1}$) is the gas solubility at measured in-situ temperature and salinity (Weiss 1974), and $pCO_{2,air}$ can be calculated from:

$$pCO_{2,air} = xCO_{2,air} \times (P_b - P_w), \quad (2)$$

where P_b (atm) is the barometric pressure from NOAA weather stations (Fig. 1), P_w (atm) is the water vapor pressure calculated using salinity and temperature (Weiss and Price 1980), and $xCO_{2,air}$ (ppm) is the mole fraction of atmospheric CO_2 in dry air. $xCO_{2,air}$ data were obtained from a Mississippi–coast CO_2 buoy (https://www.pmel.noaa.gov/co2/story/Coastal+MS).

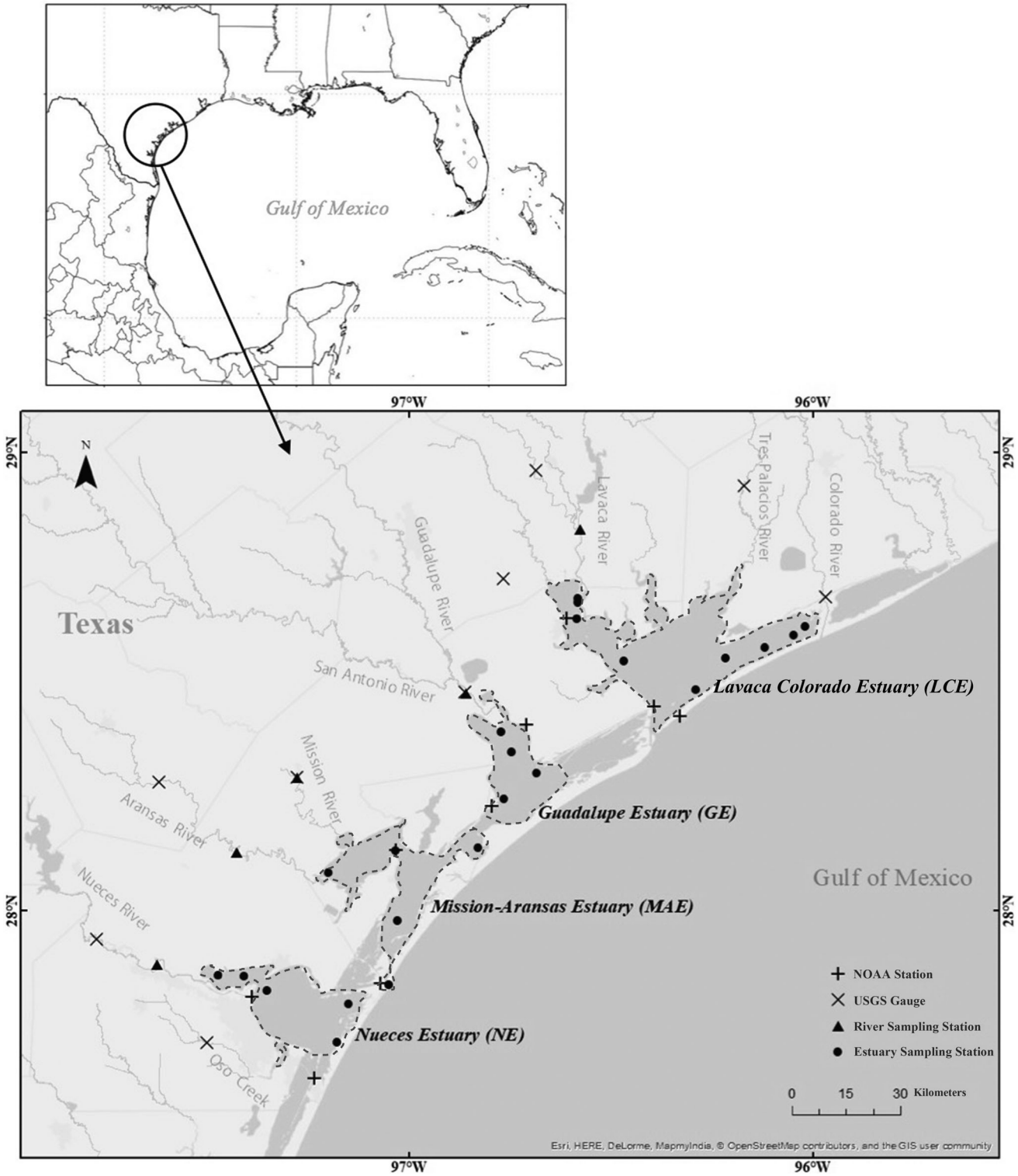

Fig. 1. Sampling stations in the nwGOM estuaries and their contributing rivers, "●" indicates estuarine stations; "▲" indicates river stations; "×" indicates USGS monitoring gauges; "+" indicates NOAA monitoring stations. Each estuary is delineated with dashed lines.

A positive flux (F value) means CO_2 degassing from the estuary to the atmosphere. Gas transfer velocity k was parameterized using wind speed and the equation from Jiang et al. (2008), which was derived from Raymond and Cole (2001) using more high wind speed (> 6 $m \cdot s^{-1}$) data:

$$k = \left(0.314 \cdot U^2 - 0.436 \cdot U + 3.99\right) \times \left(Sc_{SST}/600\right)^{-0.5}, \quad (3)$$

where U ($m\ s^{-1}$) is the wind speed at 10 m height, and Sc_{SST} is the Schmidt number of CO_2 at in-situ temperature (Wanninkhof 1992).

Area-weighted annual average CO_2 flux was calculated in each estuary following the equation:

$$F_{avg} = \frac{\sum F_i \times d_i}{\sum d_i}, \quad (4)$$

where F_{avg} is annual average CO_2 flux (in $mmol \cdot m^{-2} \cdot d^{-1}$ or $mol \cdot m^{-2} \cdot yr^{-1}$), F_i is area-weighted CO_2 flux of sampling trip i, and d_i indicates interval days in between two consecutive trips from i to $i + 1$ (Yao and Hu 2017).

Statistical analyses

According to river discharge (Fig. 2a) and corresponding estuarine salinity behavior (Table 1), the time periods were categorized into two hydrologic conditions (dry and wet). Two-way ANOVA was conducted to examine the response of the estuarine carbonate system to the dry/wet cycle and the difference between estuaries. A significant ANOVA model with significant interaction between the factors (dry/wet and estuary) indicates that the change in the dependent variable (the tested carbonate system parameter) in response to one factor depends on the level of the other factor. For example, if air–water CO_2 flux is the dependent variable and a significant interaction is found, then the effect of the dry/wet cycle on CO_2 flux varies significantly between estuaries. If a significant interaction was identified in a significant two-way ANOVA ($p < 0.05$), a follow-up

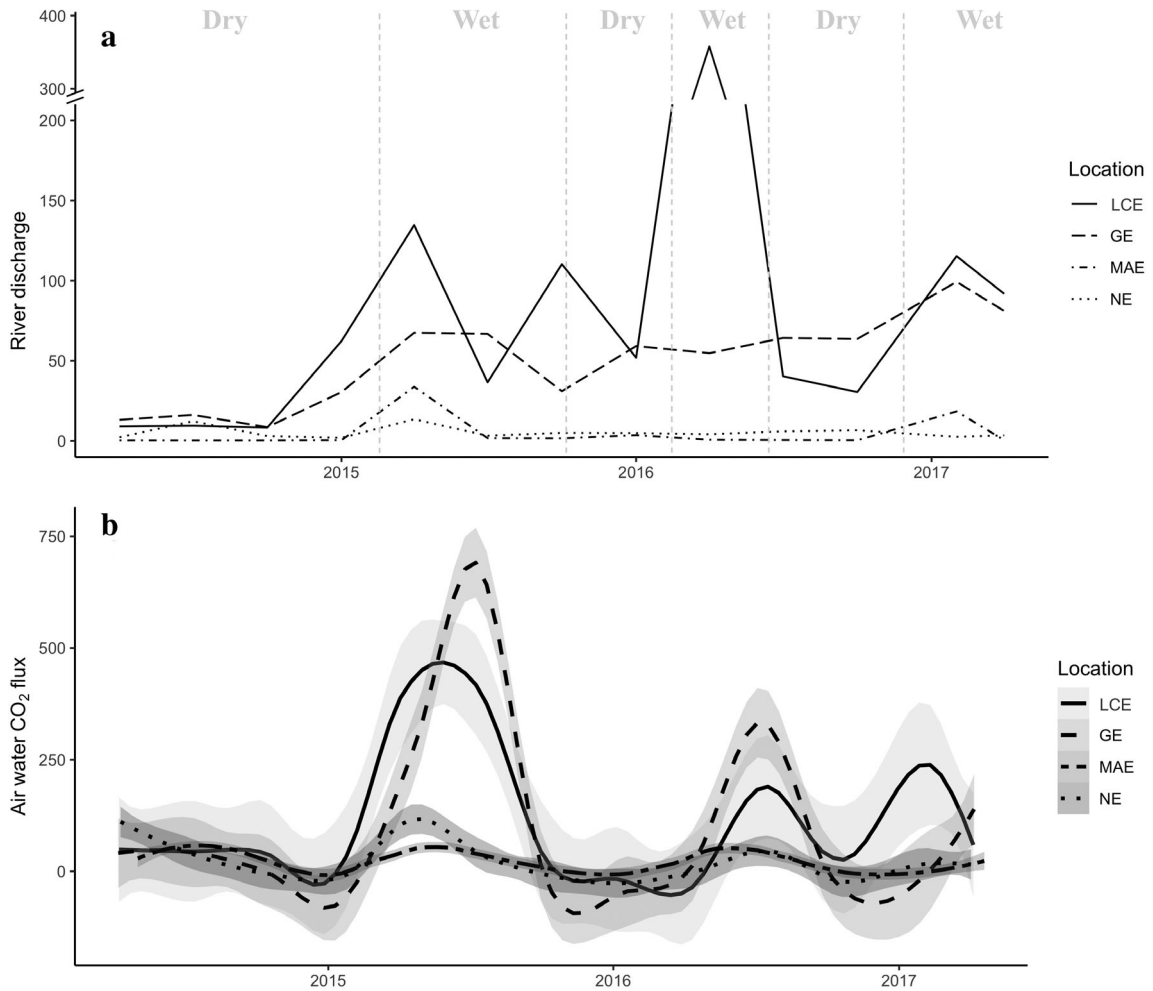

Fig. 2. River discharge (**a**) and air–water CO_2 flux (**b**) in studied estuaries, shaded areas represent stand deviation within 95% confidence (unit: $m^3 \cdot s^{-1}$ for river discharge, $mmol \cdot C \cdot m^{-2} \cdot d^{-1}$ for air–water CO_2 flux).

Table 1. Hydrologic and carbonate system parameters in four nwGOM estuaries (April 2014–February 2017).

Parameter	Estuary	Spring	Summer	Fall	Winter	Annual	Dry	Wet
Temperature (°C)	LCE	21.6 ± 1.7	30.1 ± 0.8	27.6 ± 1.0	16.0 ± 3.6	23.6 ± 5.7	22.0 ± 6.9	25.1 ± 3.9
	GE	21.0 ± 1.4	29.8 ± 0.4	27.1 ± 1.0	15.9 ± 3.8	23.3 ± 5.6	23.1 ± 6.8	23.4 ± 4.8
	MAE	23.1 ± 3.6	29.2 ± 1.2	25.3 ± 4.5	16.0 ± 3.2	24.4 ± 5.5	23.6 ± 5.5	26.8 ± 4.6
	NE	22.8 ± 1.4	30.0 ± 0.7	27.2 ± 1.9	15.3 ± 4.4	23.7 ± 5.9	22.9 ± 5.5	25.0 ± 6.3
Salinity	LCE	18.4 ± 8.4	15.8 ± 9.7	23.2 ± 5.2	19.3 ± 8.1	19.1 ± 8.4	24.3 ± 5.4	14.7 ± 8.0
	GE	14.5 ± 8.5	9.6 ± 10.7	19.6 ± 8.7	17.8 ± 8.2	15.3 ± 9.6	24.6 ± 5.5	9.5 ± 6.7
	MAE	23.3 ± 7.5	24.3 ± 12.6	26.1 ± 9.0	24.6 ± 7.0	24.6 ± 9.6	26.9 ± 8.3	18.4 ± 10.4
	NE	31.0 ± 1.9	30.1 ± 7.2	32.5 ± 4.3	31.1 ± 2.5	31.2 ± 4.3	32.9 ± 3.4	28.4 ± 4.2
DO (μmol·kg^{-1})	LCE	252.6 ± 56.6	208.5 ± 44.1	221.8 ± 21.8	335.4 ± 133.5	254.4 ± 88.5	275.2 ± 112.0	236.6 ± 56.3
	GE	271.7 ± 52.0	226.3 ± 31.7	238.5 ± 37.2	383.2 ± 138.6	279.3 ± 96.0	282.9 ± 136.5	277.1 ± 59.3
	MAE	229.4 ± 22.9	200.8 ± 24.1	222.6 ± 37.1	261.4 ± 33.9	224.0 ± 35.6	225.5 ± 37.5	219.8 ± 29.6
	NE	220.5 ± 15.7	190.9 ± 31.0	207.5 ± 27.8	270.2 ± 30.5	222.5 ± 38.8	223.1 ± 33.9	221.5 ± 45.7
pH	LCE	8.000 ± 0.285	8.057 ± 0.194	8.125 ± 0.072	8.064 ± 0.224	8.057 ± 0.219	8.100 ± 0.149	8.024 ± 0.261
	GE	8.024 ± 0.173	8.188 ± 0.100	8.293 ± 0.134	8.357 ± 0.234	8.200 ± 0.212	8.228 ± 0.222	8.184 ± 0.205
	MAE	8.007 ± 0.115	8.102 ± 0.113	8.105 ± 0.113	8.027 ± 0.095	8.066 ± 0.119	8.063 ± 0.101	8.075 ± 0.160
	NE	8.007 ± 0.092	8.141 ± 0.086	8.177 ± 0.079	8.001 ± 0.0792	8.075 ± 0.115	8.057 ± 0.103	8.104 ± 0.127
DIC (μmol·kg^{-1})	LCE	2141.9 ± 440.0	2156.7 ± 354.8	2281.6 ± 351.8	2146.6 ± 374.8	2178.6 ± 388.5	2271.0 ± 349.9	2099.5 ± 403.7
	GE	2764.4 ± 313.7	2936.1 ± 334.4	2557.1 ± 341.5	2664.5 ± 494.4	2733.1 ± 391.7	2442.3 ± 299.6	2914.9 ± 328.6
	MAE	2250.7 ± 294.4	2188.7 ± 201.1	2268.6 ± 207.5	2360.4 ± 183.7	2254.5 ± 234.5	2293.6 ± 203.8	2147.0 ± 276.8
	NE	2231.6 ± 65.7	2341.1 ± 229.6	2170.5 ± 161.0	2269.5 ± 87.5	2251.7 ± 155.5	2270.3 ± 119.1	2222.4 ± 197.5
TA (μmol·kg^{-1})	LCE	2344.7 ± 498.4	2384.7 ± 424.4	2590.0 ± 374.4	2378.5 ± 418.3	2418.3 ± 444.4	2557.8 ± 356.5	2298.8 ± 477.6
	GE	2998.6 ± 338.0	3190.5 ± 287.4	2952.6 ± 363.3	3091.2 ± 397.0	3053.6 ± 354.3	2839.1 ± 296.3	3187.7 ± 321.5
	MAE	2481.8 ± 331.9	2470.0 ± 239.3	2570.9 ± 213.6	2608.6 ± 191.6	2523.4 ± 259.3	2579.0 ± 206.6	2370.9 ± 321.7
	NE	2491.5 ± 97.2	2735.3 ± 285.2	2599.2 ± 150.9	2544.4 ± 87.9	2584.5 ± 190.2	2603.0 ± 164.8	2555.5 ± 223.1
$pCO_{2,water}$ (μatm)	LCE	682 ± 821	722 ± 467	463 ± 126	484 ± 428	595 ± 560	421 ± 164	745 ± 716
	GE	708 ± 343	873 ± 407	355 ± 58	275 ± 219	565 ± 377	364 ± 166	690 ± 417
	MAE	528 ± 192	526 ± 122	434 ± 81	382 ± 85	478 ± 143	453 ± 98	546 ± 208
	NE	475 ± 111	472 ± 77	352 ± 74	364 ± 86	420 ± 107	419 ± 89	421 ± 131

comparison of means was conducted for each level of a factor to remove the interaction. One-way ANOVAs were conducted to test for the dry condition only or the wet condition only, respectively, on whether the mean of the tested parameter varied between estuaries, and *t* tests were conducted to look for differences between wet and dry conditions in the means of the tested parameters within each estuary. The ANOVA assumptions of normality and homogeneity of variances were met, and a p value of < 0.05 was considered significant.

Results

River discharge

During our study period, significant increases in river discharge were recorded in response to storms in spring–summer 2015, spring–summer 2016, and winter–spring 2017. Wet periods in LCE and GE corresponded to the average river discharge rates of 117.4 ± 111.2 and 69.6 ± 13.4 $m^3 \cdot s^{-1}$, respectively, which were about three times of those during dry periods (i.e., 41.9 ± 37.7 and 19.9 ± 9.3 $m^3 \cdot s^{-1}$, respectively). Although total discharge was much less in MAE and NE, these estuaries also experienced spikes in river discharge that could be categorized into the same dry and wet seasons, with increases from 0.5 ± 0.6 to 10.7 ± 11.6 and 4.9 ± 3.5 to 25.0 ± 34.5 $m^3 \cdot s^{-1}$, respectively. A freshwater inflow gradient is present across these estuaries as a result of changing watershed area and precipitation/evaporation balance (Table 3); during the course of our study, we observed an order of magnitude decline in freshwater inflow from northeast (annual discharge 116.4 ± 143.7 $m^3 \cdot s^{-1}$ for LCE) to southwest (annual discharge 9.9 ± 19.2 $m^3 \cdot s^{-1}$ for NE) estuary (Fig. 2a).

Salinity

Because of the variability in freshwater inflow balance, these estuaries exhibited significant temporal and spatial differences in salinity during our study period (Tables 1 and 2). Consistent with the freshwater inflow, mean salinity was lower in the north (19.1 ± 8.4 in LCE and 15.3 ± 9.6 in GE) and higher in the south (24.6 ± 9.6 in MAE and 31.2 ± 4.3 in NE). In addition, the fall season had the highest average salinity across all estuaries, possibly because of relatively low freshwater inflow and high evaporation. Hypersalinity (salinity greater than the ocean end-member salinity, 36.5) occurred in upper MAE and NE between summer and fall 2014, which marked the end of a multiyear drought.

DO concentration

No hypoxia (defined as DO < 62.5 $\mu mol\ kg^{-1}$) was observed during our study period. DO was highest in the winter (316.2 ± 110.1 $\mu mol \cdot kg^{-1}$) and lowest in the summer (207.1 ± 37.7 $\mu mol \cdot kg^{-1}$) across all estuaries. In addition, DO decreased from northern (254.4 ± 88.5 $\mu mol\ kg^{-1}$ annual mean in LCE) to southern estuaries (223.1 ± 33.9 $\mu mol \cdot kg^{-1}$ annual mean in NE).

Estuarine carbonate system

TA and DIC varied greatly between seasons and between estuaries (Table 1, Fig. 3a,b). For example, GE had the highest average TA and DIC (3053.6 ± 354.3 and 2733.1 ± 391.7 $\mu mol \cdot kg^{-1}$, respectively), whereas LCE had the lowest average TA and DIC (2418.3 ± 444.4 and 2178.6 ± 388.5 $\mu mol \cdot kg^{-1}$, respectively). Both TA and DIC responded differently to the dry/wet cycle between estuaries, evidenced by the strong interaction of dry/wet and estuary effects in the two-way ANOVAs ($p < 0.001$, Table 2).

Table 2. Two-way ANOVA tests examine mean differences in carbonate system parameters between estuaries and between dry/wet conditions. One-way ANOVAs test for differences between estuaries in parameter means in only dry conditions or only wet conditions, and *t* tests are for differences between dry/wet conditions within each individual estuary.

	Two-way ANOVA			One-way ANOVA *p* value		*t* test, *p* value			
Parameter	Interaction	*F*	*p*	Dry	Wet	LCE	GE	MAE	NE
Temperature		2.079	0.101						
DO	**	4.772	0.003	< 0.001	< 0.001	< 0.001	0.696	0.015	0.742
Salinity	***	8.657	< 0.001	< 0.001	< 0.001	< 0.001	< 0.001	< 0.001	< 0.001
pH	***	5.513	< 0.001	< 0.001	< 0.001	0.009	0.310	0.397	0.030
DIC	***	38.590	< 0.001	< 0.001	< 0.001	< 0.001	< 0.001	< 0.001	0.123
TA	***	28.480	< 0.001	< 0.001	< 0.001	< 0.001	< 0.001	< 0.001	0.194
$pCO_{2,water}$	***	13.220	< 0.001	< 0.001	< 0.001	< 0.001	< 0.001	< 0.001	0.930
Air–water CO_2 flux	***	16.870	< 0.001	0.131	< 0.001	< 0.001	< 0.001	< 0.001	0.560
$[CO_2]_{river}$	***	9.312	< 0.001	< 0.001	< 0.001	0.406	0.329	< 0.001	0.020
$[CO_2]_{ocean}$	***	17.400	< 0.001	< 0.001	< 0.001	< 0.001	< 0.001	< 0.001	0.062
$[CO_2]_{estuarine}$	***	13.390	< 0.001	< 0.001	< 0.001	< 0.001	< 0.001	< 0.001	< 0.001

F statistic means variance of the group means, *p* value means the probability that there is no difference between tested means in the model.
***$p < 0.001$; **$p < 0.01$; *$p < 0.05$.

In LCE and MAE, TA and DIC decreased ~ 200 μmol·kg^{-1} after the flood. In GE, however, both TA and DIC increased ~ 400 μmol·kg^{-1} after the flood. In NE, neither of these parameters showed substantial changes (t test, p = 0.123 for DIC, p = 0.194 for TA; Table 2).

The seasonal mean pH across our entire study area (including all stations across all four estuaries) was highest during the fall (8.133 ± 0.118) and lowest during the spring (8.007 ± 0.176). GE had a higher pH than other estuaries, with the highest seasonal pH (8.357 ± 0.234) observed in winter. In addition, the pH variation was significant under dry/wet cycle and responded differently between estuaries (both $p < 0.001$ from one-way and two-way ANOVAs; Table 2). For example, LCE and NE experienced large variations in pH between dry and wet conditions, with pH values decreasing after a flood by an average of 0.07 (LCE, p = 0.009 from t test) and 0.05 (NE, p = 0.030 from t test), respectively. In contrast, pH remained stable in GE (p = 0.310 from t test) and MAE (p = 0.397 from t test) despite changes in flooding condition.

Estuarine pCO_2 generally decreased from northern to southern estuaries, with the highest annual mean in LCE (595 ± 560 μatm) and lowest annual in NE (420 ± 107 μatm). Despite the large temporal variability in TA and DIC in each estuary, pCO_2 displayed a consistent seasonality throughout the studied estuaries (Fig. 3c); pCO_2 was relatively high in spring and summer (567 ± 428 and 585 ± 271 μatm, respectively) and lower in fall and winter (425 ± 96 and 390 ± 236 μatm, respectively). Again, variations of pCO_2 regarded to flooding condition displayed significant spatiality between estuaries ($p < 0.001$, one-way ANOVA; Table 2). From dry to wet condition, average pCO_2 almost doubled in LCE and GE (Table 1), even though the increase was statistically significant

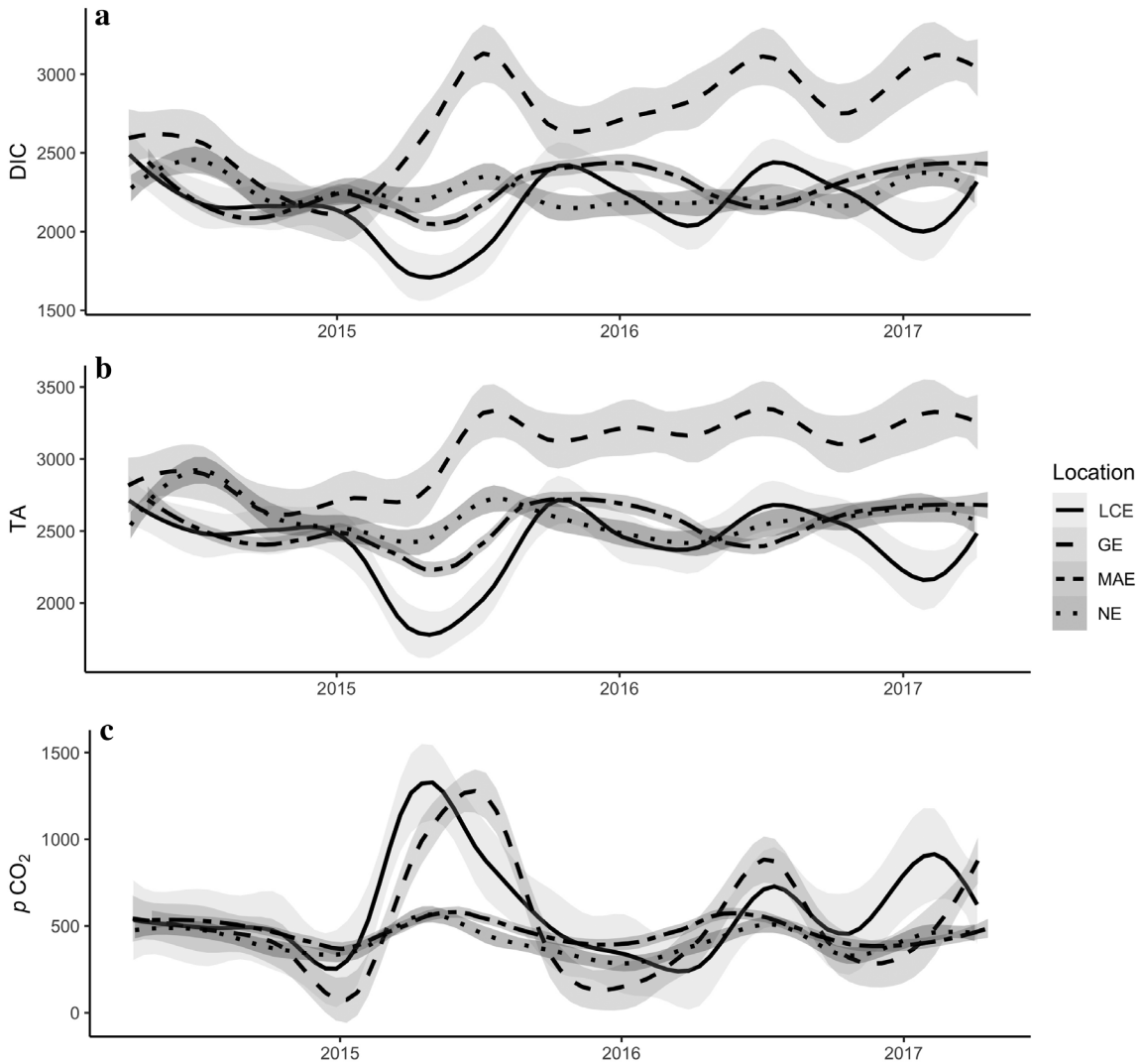

Fig. 3. Average seasonal variations of carbonate system parameters (DIC, TA, pCO_2) in studied estuaries, shaded area represents stand deviation within 95% confidence (unit: μmol·kg^{-1} for DIC and TA, μatm for pCO_2).

(t test $p < 0.001$, Table 2) pCO_2 only increased ~ 100 μatm in MAE while it showed no change in NE (t test, p = 0.930, Table 2). Thus, pCO_2 in LCE and GE had larger temporal variations than in MAE and NE (Fig. 3c).

Carbonate chemistry of river and ocean end-members

The river end-members displayed spatiotemporal variability in TA and DIC (Table 3). For example, TA and DIC concentrations were exceptionally high (3000–4500 μmol·kg^{-1}) during dry conditions at all river mouths and decreased substantially in wet conditions (both decreased 1500–3500 μmol·kg^{-1}). The only exception was NE, where minor changes in riverine TA and DIC (each ~ 200 μmol·kg^{-1} lower) were observed under wet conditions. Compared to the river end-members, the ocean end-member had little fluctuation in TA and DIC, with ~ 200 μmol·kg^{-1} decrease in wet conditions. River end-member pH was influenced by dry/wet cycle as well ($p = 0.037$ from t test, not shown), with the range significantly higher in dry (7.850–8.055) than wet condition (7.371–7.892). However, pH in the ocean end-member was only slightly greater ($p = 0.500$ from t test, not shown) in wet conditions (8.133 ± 0.058) than dry conditions (8.050 ± 0.071).

Air–water CO_2 flux

Annual mean air–water CO_2 flux decreased by one order of magnitude from north to south (Table 1), i.e., 25.6 ± 28.9 mol·C·m^{-2}·yr^{-1} in LCE and 2.7 ± 8.1 mol·C·m^{-2}·yr^{-1} in NE (Fig. 2b). In addition, CO_2 flux closely followed river discharge patterns (Fig. 2a,b). CO_2 flux was greatly elevated by increased riverine inflow, especially in LCE and GE. CO_2 flux from three of the estuaries—LCE, MAE, and NE—was similar in dry conditions (~ 20 mmol·C·m^{-2}·d^{-1}, $p = 0.131$, one-way ANOVA), although it differed significantly during wet conditions ($p < 0.001$, one-way ANOVA; Table 2). LCE and GE both experienced substantial increases in CO_2 flux from dry to wet conditions (18.3 ± 54.1 to 167.1 ± 369.1 and -0.7 ± 42.5 to 167.1 ± 369.1 mmol·C·m^{-2}·d^{-1}, respectively). In comparison, CO_2 flux in MAE showed a lesser increase from dry to wet conditions (16.9 ± 34.5 to 40.1 ± 72.0 mmol·C·m^{-2}·d^{-1}), and CO_2 flux in NE was unaffected (17.8 ± 67.2 to 20.2 ± 62.3 mmol·C·m^{-2}·d^{-1}).

Discussion

DIC and TA variations under dry and wet conditions

Our sampling period began in a drought period in 2014 with limited river discharge; in spring 2015 the drought was broken and the estuaries experienced a large increase in river discharge (Fig. 2a). For the remainder of the study duration, the entire area switched between dry and wet conditions intermittently.

Rivers in this semiarid area are known to be potentially important DIC and CO_2 sources (Butman and Raymond 2011; Zeng et al. 2011), and our study further illustrated temporal and spatial variations of riverine inputs (Fig. 4). Riverine DIC of LCE was 3174.5 ± 340.6 μmol·kg^{-1} in dry conditions

Table 3. Estuarine parameters and carbonate system of riverine and tidal inlet end-members for each estuary at dry (D) and wet (W) conditions. End-member carbonate system in each row indicates river end-member to corresponding estuary, tidal inlet is regarded as ocean end-member for all four estuaries.

Estuary	Mean depth (m)	Open water area (km^2)	Residence time (d)	Mean evaporation (km^3·yr^{-1})	Watershed area (10^3 km^2)	Mean freshwater inflow (m^3·s^{-1})	End-member carbonate system					
							Period	DIC (μmol·kg^{-1})	TA (μmol·kg^{-1})	Salinity	pH	TA/DIC
LCE	1.1	1180.6	81	1.39	130.3	107.9	D	3174.5 ± 340.6	3295.4 ± 321.4	4.5 ± 4.7	8.06 ± 0.16	1.04
							W	1548.9 ± 434.3	1546.5 ± 424.4	0.5 ± 0.7	7.51 ± 0.22	1.00
GE	1.1	561.6	39	0.78	28.1	48.3	D	4401.4 ± 570.5	4324.7 ± 306.5	0.4 ± 0.2	7.85 ± 0.08	0.98
							W	2564.8 ± 292.1	2541.2 ± 291.9	0.2 ± 0.0	7.50 ± 0.06	0.99
MAE	1.1	575.7	360	0.72	7.2	7.3	D	4661.0 ± 499.6	4705.4 ± 491.0	0.7 ± 0.1	7.87 ± 0.13	1.01
							W	1885.8 ± 255.5	1886.1 ± 230.2	0.1 ± 0.0	7.37 ± 0.01	1.00
NE	1.2	536.6	356	0.83	45.6	8.6	D	3937.5 ± 128.7	4061.9 ± 193.6	1.7 ± 1.6	7.99 ± 0.18	1.03
							W	3729.4 ± 383.7	3824.0 ± 406.9	0.4 ± 0.3	7.89 ± 0.13	1.03
Tidal Inlet	5.0	—	—	—	—	—	D	2232.4 ± 69.6	2460.0 ± 28.3	36.5 ± 0.9	8.05 ± 0.07	1.10
							W	2094.9 ± 65.2	2290.0 ± 70.7	29.5 ± 0.2	8.13 ± 0.06	1.09

D, dry period; W, wet period; —, no data.
Data are partially from Bianchi et al. (1999) and TWDB (http://www.twdb.texas.gov/surfacewater/bays/coastal_hydrology/index.asp).

(Table 3), close to the value reported in another study in this area (Zeng et al. 2011). All rivers were rich in DIC and TA compared to downstream estuaries and their ocean end-member, presumably due to high bedrock weathering and evaporation rates in this region (Zeng et al. 2011; Stets et al. 2014). However, during the wet period, intense flooding strongly diluted riverine DIC and TA (Table 3; Fig. 4b,f), this type of strong dilution effect was also observed in other studies in this region (Mooney and McClelland 2012; Montagna et al. 2018). This dilution effect varied significantly across the entire region, from the strongest in MAE (both TA and DIC were diluted more than half, ~ 2800 μmol·kg^{-1}), to the weakest in NE (diluted by 200 μmol·kg^{-1}). Therefore, the contribution of riverine biogeochemistry to estuarine carbonate chemistry may vary between estuaries and between hydrologic regimes; this highlights the need for further research on river chemistry under meteorological and hydrologic controls.

In estuaries, carbonate system variability is affected by the mixing of riverine and oceanic end-members as well as estuarine biogeochemical processes. Two end-member mixing models can be used to examine allochthonous and autochthonous dissolved constituents in order to analyze conservative/nonconservative behaviors (Bianchi 2012). Estuarine DIC and TA clearly followed salinity change (in the range of 1000–2000 μmol·kg^{-1}; Fig. 4a–h), which reveals a clear mixing scenario from river mouths to tidal inlets, when considering

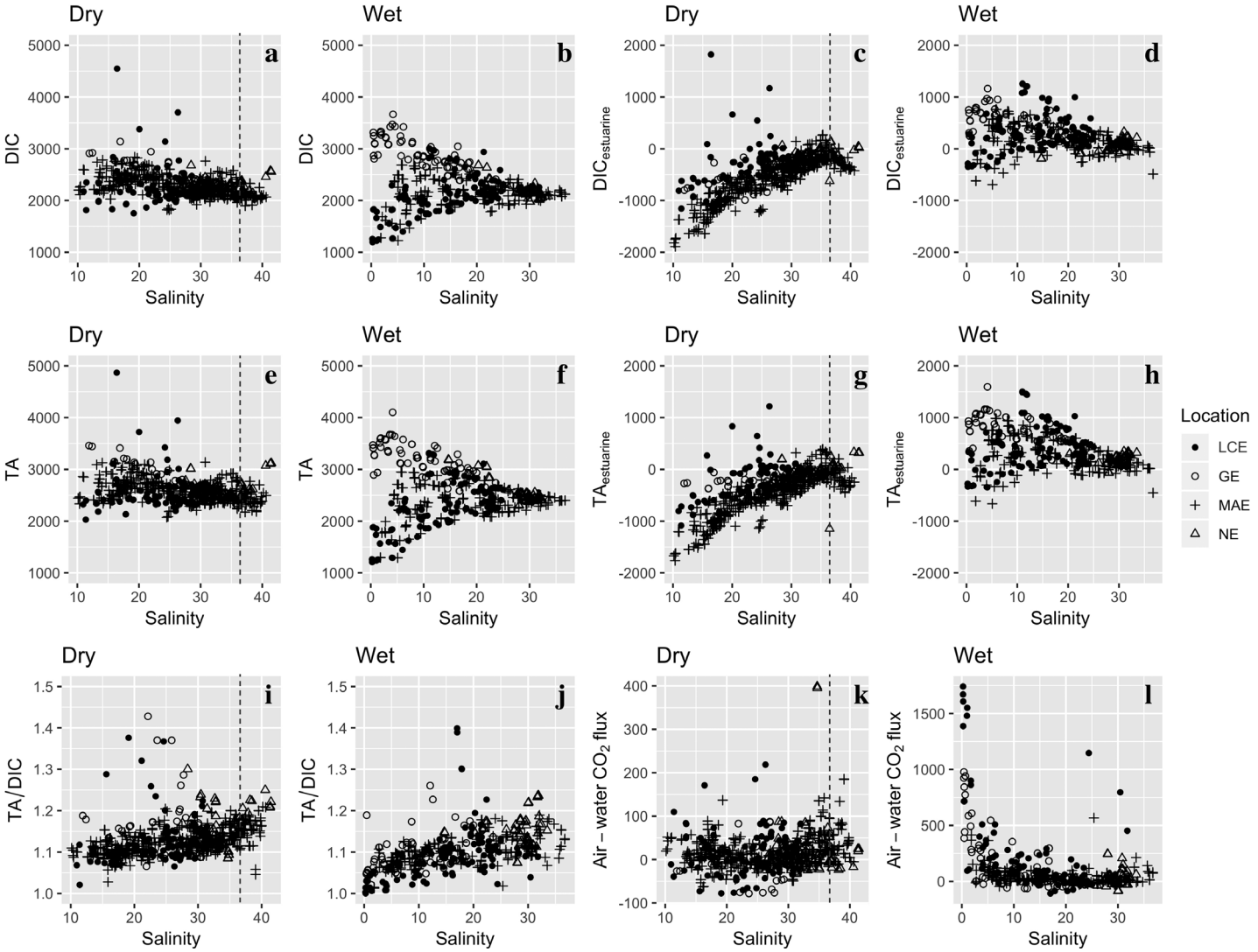

Fig. 4. DIC, TA, and CO_2 flux variations in different hydrologic conditions (i.e., wet and dry): (**a**) observed DIC in dry condition; (**b**) observed DIC in wet condition; (**c**) calculated DIC production/consumption in dry condition; (**d**) calculated DIC production/consumption in wet condition; (**e**) observed TA in dry condition; (**f**) observed TA in wet condition; (**g**) calculated TA production/consumption in dry condition; (**h**) calculated TA production/consumption in wet condition; (**i**) TA/DIC ratios in dry condition; (**j**) TA/DIC ratios in wet condition; (**k**) air–water CO_2 flux in dry condition; (**l**) air–water CO_2 flux in wet condition (unit: μmol·kg^{-1} for DIC, TA, DIC$_{estuarine}$, TA$_{estuarine}$, mmol·C·m^{-2}·d^{-1} for air–water CO_2 flux).

the uncertainties from riverine inputs (standard deviations of riverine DIC and TA values were within the range of 150∼550 μmol·kg^{-1} for all estuaries; Table 3). Therefore, we followed the method in Jiang et al. (2008) to calculate DIC change due to river–ocean mixing:

$$DIC^{r+o}_{mix/i} = \frac{(Sal_{ocean} - Sal_i) \times DIC_{river} + (Sal_i - Sal_{river}) \times DIC_{ocean}}{Sal_{ocean} - Sal_{river}}, \quad (5)$$

where ($DIC^{r+o}_{mix/i}$) is DIC due to two end-members (river and ocean) mixing at station *i*; DIC_{river} and Sal_{river} are river end-member DIC and salinity; DIC_{ocean} and Sal_{ocean} are ocean end-member DIC and Salinity; Sal_i is salinity at station *i*. Equation 5 is not applicable in estuaries under hypersaline conditions when the evaporation exceeds riverine input. Therefore, an evaporation-based equation was derived for the hypersaline water ($S > 36.5$):

$$DIC^{r+o}_{mix/i} = \frac{Sal_i}{Sal_{i-1}} \times DIC_{i-1}. \quad (6)$$

DIC_{i-1} also indicates surveyed data at station *i* from the previous field campaign, Sal_{i-1} is salinity at station *i* from the previous field campaign. Then produced/consumed DIC due to estuarine biogeochemical processes ($DIC_{estuarine}$) can be calculated as:

$$DIC_{estuarine} = DIC_i - DIC^{r+o}_{mix/i}. \quad (7)$$

DIC due to ocean mixing at station *i* (DIC^{o}_{mix}) can be calculated as

$$DIC^{o}_{mix/i} = \frac{Sal_i}{Sal_{ocean}} \times DIC_{ocean}. \quad (8)$$

Similarly, TA^{r+o}_{mix}, TA^{o}_{mix}, and $TA_{estuarine}$ can be estimated by simply replacing DIC with TA.

As a result of flooding, river-delivered organic matter was elevated, which subsequently enhanced estuarine respiration. Enhanced gross primary production due to increased nutrient input can also occur following flooding (Bruesewitz et al. 2013). Stimulated net ecosystem metabolism during wet periods contributed to large variation in $DIC_{estuarine}$ and $TA_{estuarine}$ (500–1000 μmol·kg^{-1}, where positive values are net production and negative values are net consumption, Fig. 4d, h), especially in the upper estuaries. The positive $DIC_{estuarine}$ and $TA_{estuarine}$ values found for the majority of measurements during wet periods represented a heterotrophic state coupled with other biogeochemical processes. For example, ΔDIC vs. ΔTA (Δ represents the difference between values from two consecutive trips; Fig. 5) provided useful insights on drivers of DIC and TA dynamics (Sippo et al. 2016; Liu 2017). The majority of ΔDIC/ΔTA ratios in wet periods (Fig. 5) were ratios that would be expected for a combination of aerobic respiration (–0.2), denitrification (0.9), and carbonate dissolution (2). All three processes have been well studied in this area during wet periods (Russell et al. 2006; Bruesewitz et al. 2013; Murgulet et al. 2018). This overall net heterotrophy also favored CO_2 emission (seen as positive air–water CO_2 flux in Fig. 4l). In addition, ΔDIC/ΔTA change in LCE and MAE indicated a strong dilution effect during a large flood (slope close to 1.2 when $S < 5$; Fig. 5), which was consistent with their riverine DIC and TA declines in wet conditions.

In contrast, a small number of negative $DIC_{estuarine}$ and $TA_{estuarine}$ near river mouths ($S < 10$, Fig. 4d,h) suggested a net consumption resulting from the transition to net autotrophy. Such consumption extended through the following period of flood relaxation. During dry conditions DIC and TA consumption could amount to a maximum of –2000 μmol·kg^{-1}, particularly near the river mouth (Fig. 4c,g), and in these conditions, ΔDIC/ΔTA (Fig. 5) was mainly influenced by photosynthesis (–0.2), carbonate precipitation (2), and nitrification (–∞). Past studies in this region have shown high sustained levels of phytoplankton (Reyna et al. 2017) and particulate organic carbon (Mooney and McClelland 2012), indicating that autotrophy is favored. An and Joye (2001) also reported that nitrification is stimulated (10-fold higher, up to 12.85 mmol·m^{-2}·d^{-1}) by benthic photosynthesis in a similar shallow estuary—Galveston Bay—adjacent to this region. It is reasonable to expect such enhanced nitrification occurred in the water column when phytoplankton accumulated after flood events. On the other hand, as all estuaries support commercial oyster production, carbonate precipitation may be an important process that could decrease both $DIC_{estuarine}$ and $TA_{estuarine}$ under dry conditions (Murgulet et al. 2018). Detailed explorations of C and N co-variation in response to hydrologic change are necessary to better understand the biogeochemistry at play rather than solely relying on stoichiometry.

Upper MAE and NE experienced hypersalinity (salinity exceeded the average ocean end-member salinity, $S > 36.5$; Fig. 4a,c,e,g,i,k) during May 2014 and October 2014. At hypersalinity CO_2 effluxes were variables but elevated ($S > 35$, Fig. 4k). This is consistent with our previous study, which revealed that evaporating estuarine water holds less dissolved CO_2; and CO_2 efflux is significant under high wind speeds (Yao and Hu 2017). This CO_2 efflux should contribute to DIC loss ($DIC_{estuarine} < 0$; Fig. 4c). Consistent with a previous study that demonstrated net alkalinity loss at hypersalinity (Hu et al. 2015; Murgulet et al. 2018), we observed TA consumption with elevated salinity under dry conditions (Fig. 4e, g). $TA_{estuarine}$ was expected to be negative in hypersaline conditions, as elevated ammonium release (up to 100 μmol·m^{-2}·h^{-1}) and sulfide accumulation (∼ 40 μmol·kg^{-1}) has been observed at the sediment–water interface in NE as a result of enhanced dissimilatory nitrate reduction to ammonium (Gardner et al. 2006). No hypoxia was observed

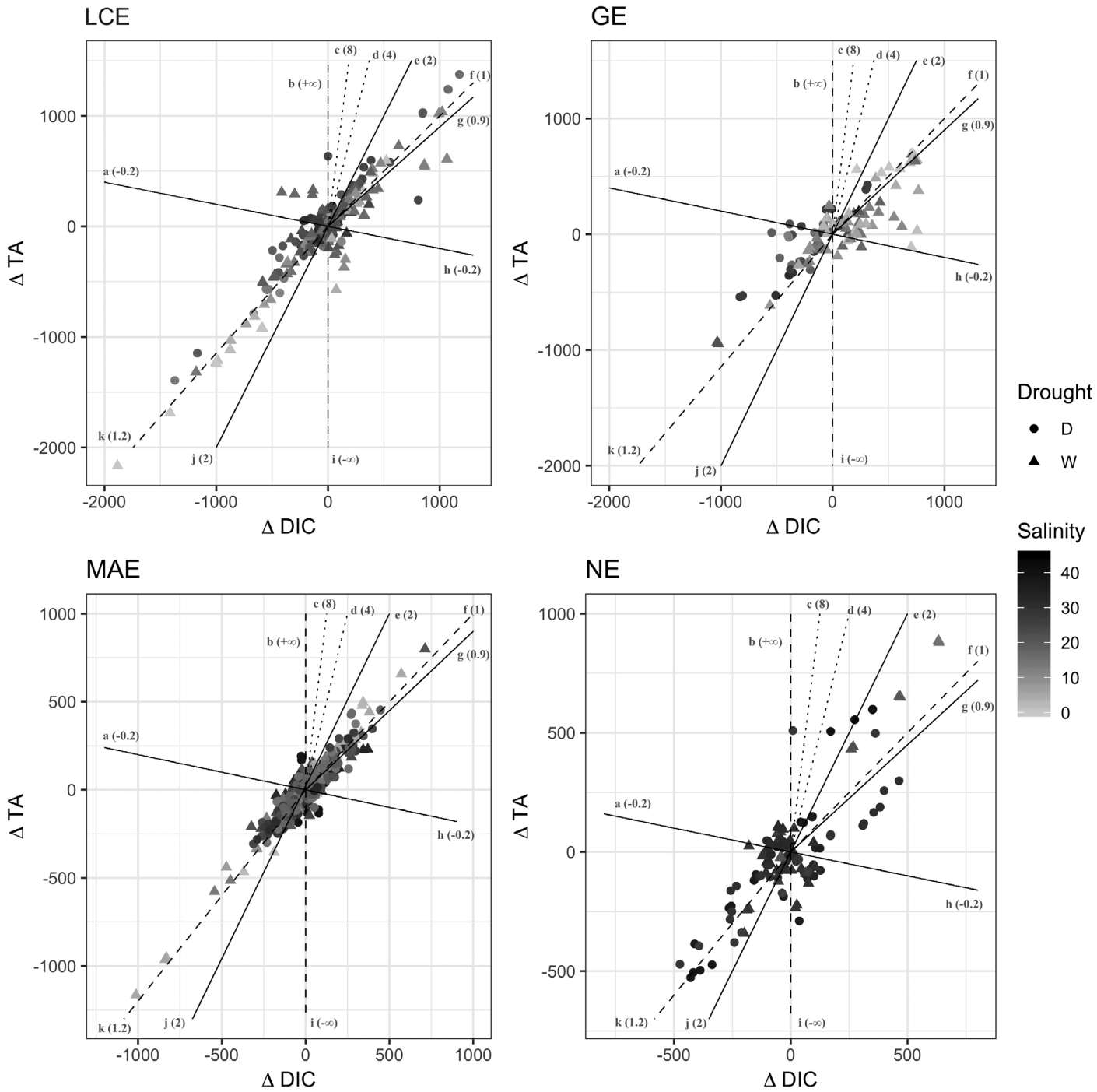

Fig. 5. △DIC vs. △TA in each estuary. The straight lines indicate different biogeochemical processes that will lead to DIC and TA changes with various fixed ratios (values in bracket indicate the ratios/slopes, Liu 2017; Sippo et al. 2016). (**a**) Photosynthesis; (**b**) hydrolysis; (**c**) iron reduction; (**d**) manganese reduction; (**e**) calcium carbonate dissolution; (**f**) sulfate reduction; (**g**) denitrification; (**h**) aerobic respiration; (**i**) nitrification/sulfide oxidation; (**j**) calcium carbonate precipitation; (**k**) dilution/evaporation. (unit: μmol·kg^{-1}).

in this study, indicating that nitrification and sulfide oxidation may have occurred in the water column. However, further studies that associate nitrogen and sulfur cycles with carbonate chemistry would be necessary fully reveal their roles.

River-borne, ocean-borne, and estuarine-generated CO_2

We use $[CO_2]_{ocean}$, $[CO_2]_{river}$, and $[CO_2]_{estuarine}$ to represent ocean-borne $[CO_2]$, river-borne $[CO_2]$, and estuarine-produced $[CO_2]$, respectively. Because aqueous CO_2 ($[CO_2]$) does not mix conservatively, $[CO_2]_{ocean}$ is the aqueous CO_2

concentration of the ocean end-member if these were diluted by freshwater with zero DIC, calculated by DIC^{o}_{mix} and TA^{o}_{mix} (see Eq. 8). $[CO_2]_{river}$ is the difference between $[CO_2]$ due to mixing and $[CO_2]_{ocean}$ (Jiang et al. 2008):

$$[CO_2]_{river} = [CO_2]^{r+o}_{mix/i} - [CO_2]_{ocean}. \quad (9)$$

$[CO_2]^{r+o}_{mix/i}$ is the aqueous CO_2 concentration if conservative mixing occurred between river and ocean end-members, calculated using DIC^{r+o}_{mix} and TA^{r+o}_{mix}:

$$[CO_2]_{estuarine} = [CO_2]_i - [CO_2]^{r+o}_{mix/i}, \quad (10)$$

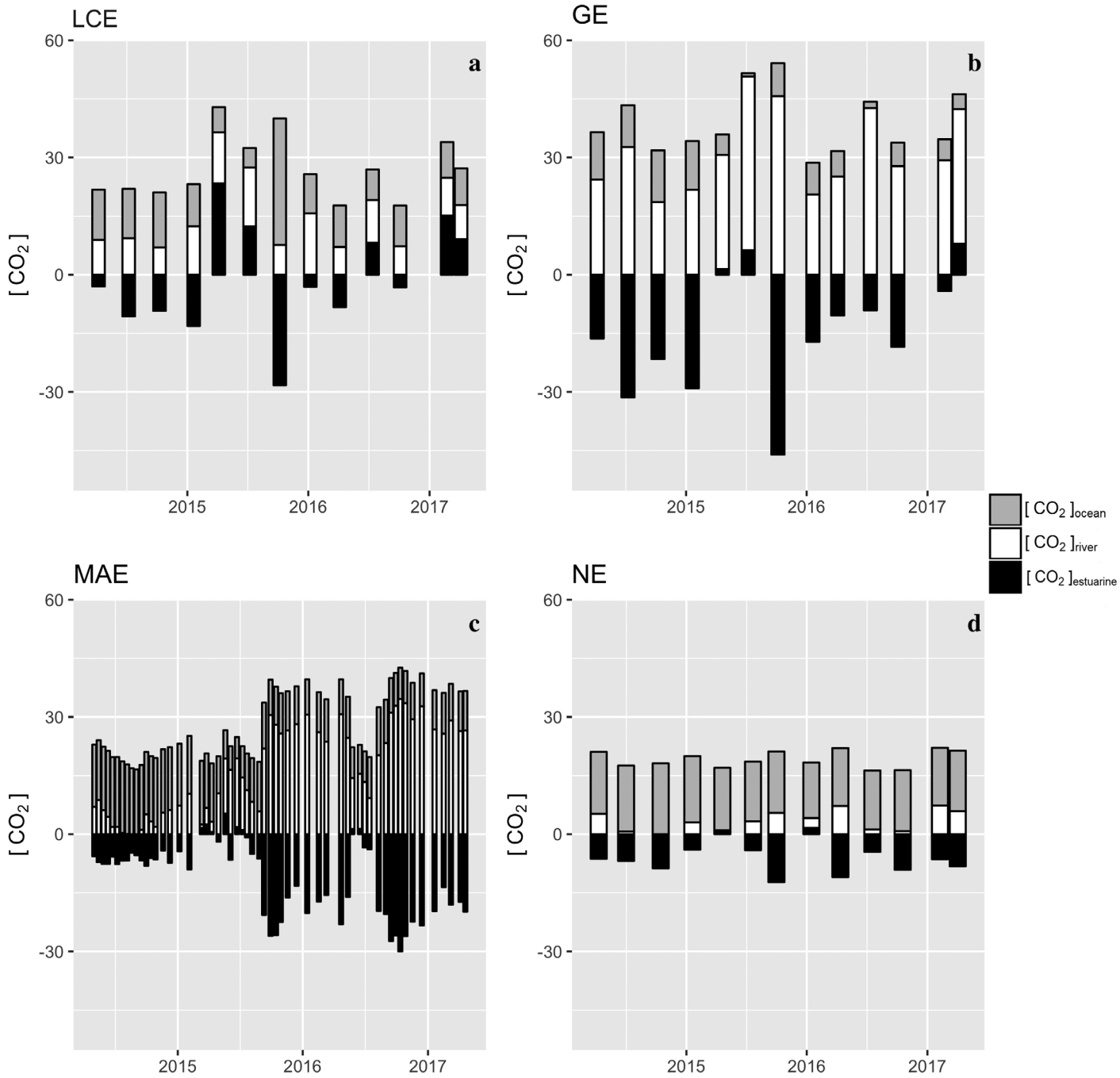

Fig. 6. Area-weighted categorized aqueous CO_2 concentrations ($[CO_2]_{river}$, $[CO_2]_{ocean}$, $[CO_2]_{estuarine}$) in studied estuaries. (unit: μmol·kg^{-1}).

$[CO_2]_{estuarine}$ is aqueous CO_2 due to estuarine biogeochemical reactions. $[CO_2]_i$ is actual aqueous CO_2 concentration based on field data.

As aqueous CO_2 concentrations were subject to water temperature changes, all $[CO_2]$ categories were normalized to the average temperature (23.9°C) to eliminate the thermal effect (Jiang et al. 2008). TA in estuarine waters contains noncarbonate species, which would lead to an underestimation of CO_2 concentration if using TA and DIC as the input variables in CO_2 system speciation calculations; for example, including 50 μmol·kg^{-1} (an average ΔTA from our surveys) of noncarbonate alkalinity in the TA input decreases calculated $[CO_2]$ by 3.0 μmol·kg^{-1} at salinity 23.3 and temperature 23.9°C (all average values). Nevertheless, this exercise would still be useful for qualitatively tracking the dynamic of CO_2 flux in the aquatic system, especially for $[CO_2]$ mixing from multiple sources (Jiang et al. 2008).

Area-weighted average $[CO_2]$ for each sampling trip was calculated (arithmetic mean of stations in each bay, multiplied by bay area), all three $[CO_2]$ categories displayed significant temporal and spatial trends (Fig. 6, Table 2). When $[CO_2]_{river}$ accounted for more than 50% of $[CO_2]$ the scenario was considered river-dominated, and when $[CO_2]_{ocean}$ accounted for more than 50% of $[CO_2]$ the scenario was considered ocean-dominated. These estuaries displayed scenarios ranging between river-dominated and ocean-dominated, mostly depending on hydrologic conditions. For instance, river discharge was two orders of magnitude lower in NE and MAE than LCE and GE (Fig. 2a). This directly led to a $[CO_2]_{river}$ that was 9.2 times higher annually in GE (30.5 ± 9.1 μmol·kg^{-1}) than NE (3.3 ± 2.7 μmol·kg^{-1}) and a $[CO_2]_{ocean}$ 53.8% lower annually in GE (7.3 ± 4.0 μmol·kg^{-1}) than NE (15.8 ± 1.1 μmol·kg^{-1}). As a result, GE was river-dominated throughout the study duration (Fig. 6b), whereas NE was clearly

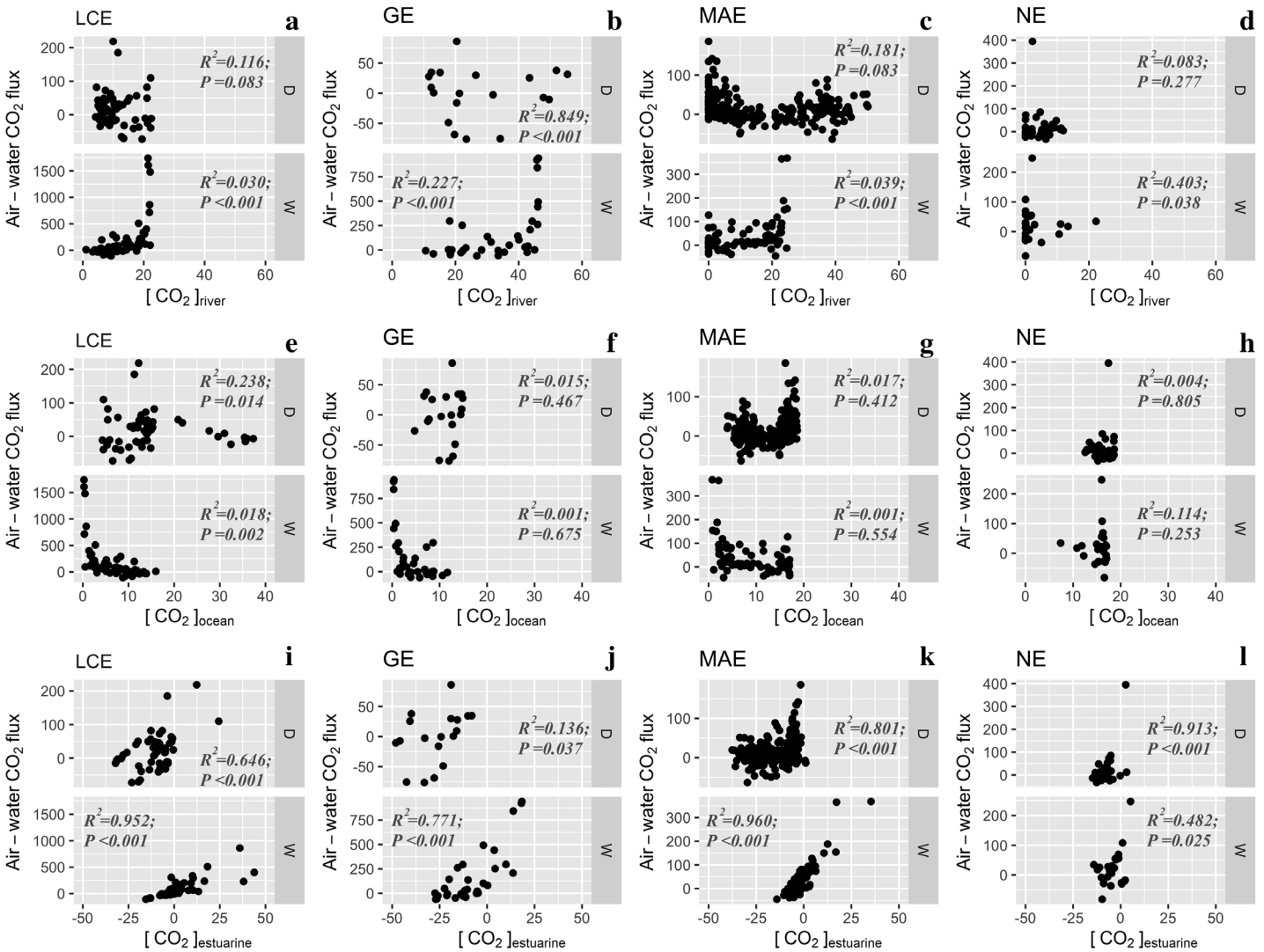

Fig. 7. Correlation analyses between categorized aqueous $[CO_2]_x$ and air–water CO_2 flux in studied estuaries in wet and dry conditions. D, dry condition; W, wet condition (unit: μmol·kg^{-1} for $[CO_2]_x$; mmol·C·m^{-2}·d^{-1} for air–water CO_2 flux).

ocean-dominated throughout the study duration (Fig. 6d). NE likely maintained the ocean-dominated state due to anthropogenic intervention (i.e., dam construction and river fragmentation; Murgulet et al. 2016), which limit freshwater inflow and result in a more negative freshwater balance (Montagna et al. 2012). LCE and MAE exhibited both river-dominated and ocean-dominated scenarios depending on changing hydrologic conditions (Fig. 6a,c). The relative contribution of $[CO_2]_{estuarine}$ differed significantly between wet and dry conditions, while $[CO_2]_{river}$ only differed between wet and dry conditions in MAE and NE and $[CO_2]_{ocean}$ only differed between wet and dry conditions in NE (*t* test $p < 0.05$, Table 2).

Interestingly, all four estuaries responded differently to changes in flooding (Fig. 7). As expected, CO_2 flux was significantly related to $[CO_2]_{river}$ during flooding throughout the region (Fig. 7a–d). During the river-dominated state, CO_2 effluxes increased exponentially with elevated $[CO_2]_{river}$ in LCE, GE, and MAE (wet condition of Fig. 7a–c). A previous study suggested that river-borne CO_2 ventilation could contribute to such exponential increase of CO_2 emission in river-dominated estuaries (Borges et al. 2006). Borges et al. (2006) also suggested that river-borne CO_2 ventilation decreases exponentially with longer water residence, but even NE, where ocean-dominated condition prevailed most of the time, $[CO_2]_{river}$ still contributed to CO_2 flux in wet conditions ($R^2 = 0.403$, $p = 0.038$, Fig. 7d). However, relatively low correlation between $[CO_2]_{river}$ and CO_2 flux (for most estuaries $R^2 < 0.2$ both in dry and wet conditions; Fig. 7a–d) indicated that ventilation of river-borne CO_2 was not the main control on CO_2 flux across our study area.

$[CO_2]_{estuarine}$, an indicator of estuarine biogeochemical processes, played a crucial role in determining CO_2 flux of this region (Fig. 7i–l). For example, CO_2 flux in MAE was primarily controlled by $[CO_2]_{estuarine}$ in both dry and wet conditions ($R^2 = 0.801$ and 0.960, respectively; $p < 0.001$ for both, Fig. 7k). Likewise, $[CO_2]_{estuarine}$ contributed significantly to CO_2 flux in all of our studied estuaries ($p < 0.05$ for all cases; Fig. 7i,j,l), especially during wet periods. Due to long residence times (40–360 d; Bianchi et al. 1999), pulses of freshwater inflow can generate profound influences in nwGOM estuarine systems, that is, CO_2 flux was elevated during flooding, but on an annual scale CO_2 flux was relatively depressed, potentially because nutrient input from floods stimulated phytoplankton growth. Both $DIC_{estuarine}$ and categorized $[CO_2]$ revealed the strongest autotrophy during a mild drought after a major storm ($DIC_{estuarine}$ ranged −2000 to 1000 $\mu mol \cdot kg^{-1}$ in salinity 10–20, Fig. 4c, and area-weighted $[CO_2]_{estuarine}$ ranged −15 to 45 $\mu mol \cdot kg^{-1}$ in Fall 2015, Fig. 6). The autotrophy-dominated drought period yielded a similar CO_2 flux among LCE, MAE, and NE ($\sim$ 18.0 $mmol \cdot C \cdot m^{-2} \cdot d^{-1}$), and it yielded a CO_2 sink (−0.7 ± 42.5 mmol·C·m⁻2·d⁻1) in GE despite GE's high river discharge relative to MAE and NE.

Even though ocean-dominated scenarios were identified in LCE, MAE, and NE (Fig. 6a,c,d), the lack of correlation

Table 4. Annual and seasonal air–water CO_2 fluxes in U.S. estuaries.

	Average air–water CO_2 flux (unit: $mol \cdot C \cdot m^{-2} \cdot yr^{-1}$ for annual; $mmol \cdot C \cdot m^{-2} \cdot d^{-1}$ for seasonal)						
Estuary*	Annual	Spring (mar-may)	Summer (Jun–Aug)	Fall (Sep–Nov)	Winter (Dec–Feb)	Latitude (°N)	References
Altamaha Sound[b]	26.8	57.8	127.0	79.7	28.5	31.3	Jiang et al. (2008)
Delaware[a]	2.4 ± 4.8	−13.7 ± 16.4	13.4 ± 22.2	2.7 ± 6.6	15.6 ± 5.2	38.9	Joesoef et al. (2015)
Florida Bay[b]	1.7					25.0	Millero et al. (2001)
Great Bay[c]	3.6					43.1	Hunt et al. (2010)
Kaneohe Bay[b]	1.5					21.4	Fagan and Mackenzie (2007)
Kennebec[c]	−0.5	22.5	22.0	−0.2	−49.6	43.8	Hunt et al. (2013)
Little Bay Estuary[c]	4.0	−5.1	33.0	3.9		43.1	Hunt et al. (2010)
New River Estuary[a]	−0.2 to 2.0					34.5–34.7	Crosswell et al. (2017)
Neuse River[a]	4.7	1.73	−0.84	38.4	12.1	35.0	Crosswell et al. (2012)
San Francisco estuary[b]	0.4		1.8		0.5	37.7	Peterson (1979)
Shark River[a]	16.0					25.2	Koné and Borges (2008)
Shark River[a]	36.1						Ho et al. (2016)
York River[b]	5.6	10.0	29.0	16.7	6.5	37.2	Raymond et al. (2000)
LCE[a]	25.6 ± 28.8	118.5 ± 390.0	190.6 ± 317.6	24.4 ± 44.5	53.5 ± 178.7	27.8–28.1	This study
GE[a]	35.9 ± 24.2	98.2 ± 136.9	343.2 ± 365.1	−6.0 ± 9.2	−31.3 ± 39.8		
MAE[a]	6.9 ± 6.5	33.8 ± 66.1	42.1 ± 47.2	11.5 ± 22.2	−9.4 ± 23.8		
NE[a]	2.7 ± 8.1	55.3 ± 101.2	26.6 ± 24.0	−12.7 ± 24.7	−6.4 ± 21.4		

*Superscripts a, b, and c indicate different tidal types: a, microtidal estuary; b, macrotidal estuary; c, mesotidal estuary.

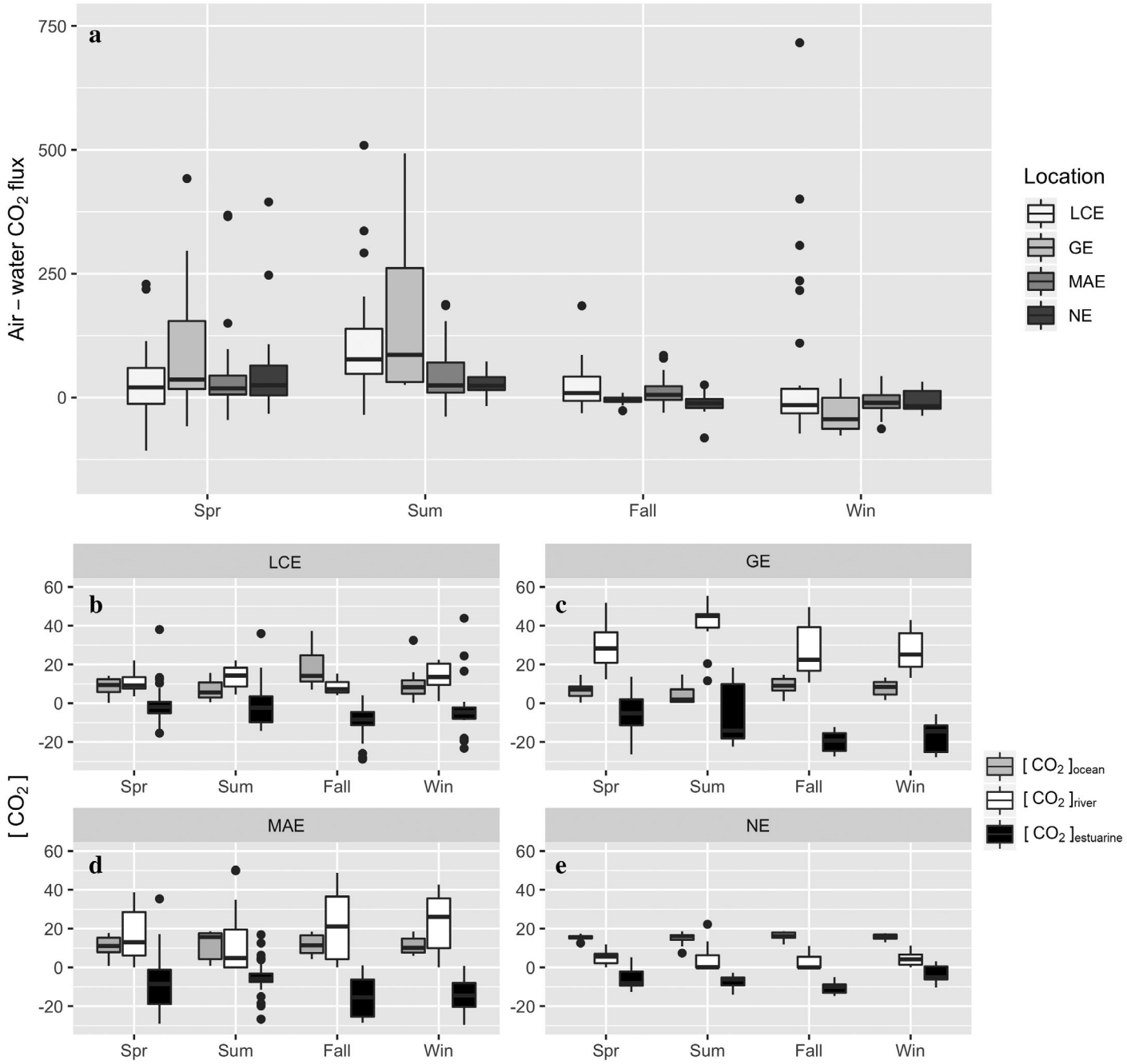

Fig. 8. Seasonality of air–water CO_2 flux and categorized aqueous CO_2 in studied estuaries (unit: μmol·kg^{-1} for $[CO_2]_x$; mmol·C·m^{-2}·d^{-1} for air–water CO_2 flux).

between $[CO_2]_{ocean}$ and CO_2 flux suggested that $[CO_2]_{ocean}$ exerted the weakest control on CO_2 flux in this area (Fig. 7e–h). The only exception was in LCE, where $[CO_2]_{ocean}$ was significantly correlated with CO_2 flux (p = 0.014 for dry and p = 0.002 for wet period; Fig. 7e). This exception may be caused by the decrease in organic matter with decreasing riverine input (seen as lower $[CO_2]_{river}$; Fig. 6a), which subsequently led to lower $[CO_2]_{estuarine}$ (Fig. 6a). $[CO_2]_{estuarine}$ was the most important contributor to CO_2 flux in LCE (R^2 = 0.646 and 0.952 for dry and wet conditions, respectively; Fig. 7i).

Annual and seasonal CO_2 flux

During the 3 years of this study, the nwGOM estuaries acted as an overall CO_2 source to the atmosphere (Table 4; Fig. 2). By applying an area-weighted average (Eq. 4), annual air–water CO_2 flux from the entire system was

16.6 ± 17.1 mol·C·m^{-2}·yr^{-1}, with approximately an order of magnitude decline from the northeast to southwest (i.e., from 25.6 mol·C·m^{-2}·yr^{-1} in LCE to 2.7 mol·C·m^{-2}·yr^{-1} in NE, Table 4). This region-wide flux estimate agrees with an earlier estimation of CO_2 flux of global lagoonal estuaries (17.3 ± 16.6 mol·C·m^{-2}·yr^{-1}; Laruelle et al. 2010). On the other hand, Chen et al. (2013) estimated that average CO_2 flux in North American estuaries is 2.2 mol·C·m^{-2}·yr^{-1}, although their study was mostly based on U.S. east coast estuaries. Furthermore, annual CO_2 flux in MAE during these 3 years was 6.9 ± 6.5 mol·C·m^{-2}·yr^{-1}; our previous study estimated a much higher CO_2 flux in MAE (12.4 ± 3.3 mol·C·m^{-2}·yr^{-1}), although that study only spanned May 2014 to April 2015, a period of drought that preceded a large freshwater discharge event in April 2015 (Yao and Hu 2017). In the longer time series that we present in this study, it is likely that elevated freshwater inflow delivered nutrients and subsequently enhanced autotrophic production and reduced CO_2 emission, especially when MAE returned to an ocean-dominated condition following the flooding. Moreover, wind speeds can play a crucial role in estuarine CO_2 flux. This windy and shallow environment seems to favor fast air–water gas exchange even though average estuarine pCO_2 was not much greater than atmospheric pCO_2 (Table 1). We want to note that we used a wind-dependent function that was originally derived from the open ocean to calculate gas transfer velocity (Eq. 3) (Wanninkhof 1992). There is not yet a consensus on the parameterization of estuarine gas transfer velocity, nor have there been direct measurements of this velocity in our study area; therefore, a better gas transfer velocity measurement is crucial to developing more accurate CO_2 flux estimates in future estuarine research (Raymond and Cole 2001; Jiang et al. 2008; Rosentreter et al. 2017). Regardless, the comparison between the two data series with different temporal coverages highlights the dynamic nature of estuarine environments.

Not only did estuarine CO_2 flux in the nwGOM vary spatially, it also exhibited strong seasonality (Table 4; Fig. 8a). In this study, strong CO_2 efflux in spring and summer months weakened and transitioned to influx in fall and winter (Table 4; Fig. 8a). Large riverine inflows from three major freshwater discharge events and the simultaneous high wind speeds (data not shown) resulted in the strong CO_2 efflux in spring and summer. After the flood influence subsided, net autotrophy (as demonstrated by widespread high pH, low pCO_2, and negative $[CO_2]_{estuarine}$ (Table 1; Fig. 6) significantly reduced the fall CO_2 efflux (Fig. 8a). Water temperature decreased from fall to winter along with pCO_2 and CO_2 flux. A temperature decline of $\sim 10^{\circ}$C could result in ~ 200 μatm decrease in pCO_2 in MAE (Yao and Hu 2017). Together, the lowered pCO_2 and the lowest seasonal wind speed resulted in a moderate to weak CO_2 sink in these estuaries in the winter (Fig. 8a). A larger decline in winter pCO_2 was expected in the more northern estuaries LCE and GE since this thermal effect was also salinity-related, that is, temperature-normalized pCO_2 would decrease in low-salinity region with smaller temperature dependence ($\partial \ln pCO_2/\partial T$) (Joesoef et al. 2015). Therefore, the CO_2 flux reversal in winter appears to be controlled more by weather (temperature and wind speed) than biological activities. For example, CO_2 flux dropped ~ 20 mmol C·m^{-2}·d^{-1} in GE and MAE from fall to winter (Table 4), yet $[CO_2]_{river}$ and $[CO_2]_{estuarine}$ were relatively the same (Fig. 8c,d). While the thermal effect became important in winter months, hydrologic change remained the most important to the system; this was demonstrated in LCE, where (despite high variations) elevated freshwater inflow ($[CO_2]_{river}$ increased from 8.3 ± 3.1 to 14.3 ± 6.5 μmol·kg^{-1}; Fig. 8b) and caused the seasonal CO_2 efflux to double from fall to winter (from 24.4 ± 44.5 to 53.5 ± 178.7 mmol C·m^{-2}·d^{-1}, Table 4).

Conclusions

Our study covered an extreme range of hydrologic conditions, from drought to flooding, and estuaries that ranged from river-dominated to ocean-dominated. In general, nwGOM estuaries LCE, GE, MAE, and NE are a net CO_2 source to the atmosphere on an annual scale with large temporal and spatial variations. About an order of magnitude decline in annual average air–water CO_2 flux was observed from northeast to southwest along the coastline. Substantial CO_2 degassing due to large freshwater inflow events and high wind conditions occurred in spring and summer, and CO_2 flux switched to a weak CO_2 sink in fall and winter. Hydrologic and meteorological influences, such as river discharge, wind speed, and water temperature played important roles in driving CO_2 fluxes. Both negative $DIC_{estuarine}$ and $[CO_2]_{estuarine}$ implied overall autotrophy after summer flooding, despite high initial river-borne CO_2 enrichment. In addition, CO_2 emission was elevated by evaporation and high wind speeds, which further led to net DIC consumption in hypersaline water. Overall, our findings indicate that estuarine carbon cycle variability is highly dependent on estuarine hydrologic condition, and more comprehensive studies should be done to further assess this effect in a broader context.

References

Abril, G., G. Abril, S. Bouillon, F. Darchambeau, C. R. Teodoru, T. R. Marwick, F. Tamooh, F. O. Omengo, N. Geeraert, L. Deirmendjian, P. Polsenaere, and A. V. Borges. 2015. Technical note: Large overestimation of pCO_2 calculated from pH and alkalinity in acidic, organic-rich freshwaters. Biogeosciences **12** 67–78. doi:10.5194/bg-12-67-2015

An, S., and S. B. Joye. 2001. Enhancement of coupled nitrification-denitrification by benthic photosynthesis in shallow estuarine sediments. Limnol. Oceanogr. **46** 62–74. doi:10.4319/lo.2001.46.1.0062

Bauer, J. E., W. J. Cai, P. A. Raymond, T. S. Bianchi, C. S. Hopkinson, and P. A. Regnier. 2013. The changing

carbon cycle of the coastal ocean. Nature **504** 61–70. doi:10.1038/nature12857

Bianchi, T. S. 2012. Estuarine chemistry. In, p. 39–83. *In* J. W. Day, B. C. Crump, W. M. Kemp and A. Yáñez-Arancibia [eds.], Estuarine ecology. Wiley-Blackwell.

Bianchi, T. S., J. R. Pennock, and R. R. Twilley. 1999. Biogeochemistry of Gulf of Mexico estuaries. John Wiley & Sons.

Borges, A. V., L. S. Schiettecatte, G. Abril, B. Delille, and F. Gazeau. 2006. Carbon dioxide in European coastal waters. Estuar. Coast. Shelf Sci. **70** 375–87. doi:10.1016/j.ecss.2006.05.046

Boynton, W., L. Murray, J. Hagy, C. Stokes, and W. Kemp. 1996. A comparative analysis of eutrophication patterns in a temperate coastal lagoon. Estuaries **19** 408–21. doi:10.2307/1352459

Bruesewitz, D. A., W. S. Gardner, R. F. Mooney, L. Pollard, and E. J. Buskey. 2013. Estuarine ecosystem function response to flood and drought in a shallow, semiarid estuary: Nitrogen cycling and ecosystem metabolism. Limnol. Oceanogr. **58** 2293–309. doi:10.4319/10.2013.58.6.2293

Butman, D., and P. A. Raymond. 2011. Significant efflux of carbon dioxide from streams and rivers in the United States. Nat. Geosci. **4** 839–42. doi:10.1038/ngeo1294

Carter, B. R., J. A. Radich, H. L. Doyle, and A. G. Dickson. 2013. An automated system for spectrophotometric seawater pH measurements. Limnol. Oceanogr. - Meth. **11** 16–27. doi:10.4319/lom.2013.11.16

Chen, C. T. A., T. H. Huang, Y. C. Chen, Y. Bai, X. He, and Y. Kang. 2013. Air–sea exchanges of CO_2 in the world's coastal seas. Biogeosciences **10** 6509–44. doi:10.5194/bg-10-6509-2013

Cromwell, J. E. 1971. Barrier coast distribution: a world-wide survey. In Abstracts, Second Coastal and Shallow Water Research Conference. Los Angeles, California: US Office of Naval Research Geography Program, Univ. Press, Univ. of Southern California.

Crosswell, J. R., M. S. Wetz, B. Hales, and H. W. Paerl. 2012. Air–water CO_2 fluxes in the microtidal Neuse River Estuary, North Carolina. J. Geophys. Res. Ocean **117** C08017. doi:10.1029/2012jc007925

Crosswell, J. R., I. C. Anderson, J. W. Stanhope, B. Van Dam, M. J. Brush, S. Ensign, M. F. Piehler, B. McKee, M. Bost, and H. W. Paerl. 2017. Carbon budget of a shallow, lagoonal estuary: Transformations and source-sink dynamics along the river-estuary-ocean continuum. Limnol. Oceanogr. **62** S29–S45. doi:10.1002/lno.10631

Dickson, A. G. 1990. Standard potential of the reaction: $AgCl(s) + 12H_2(g) = Ag(s) + HCl(aq)$, and and the standard acidity constant of the ion HSO_4^- in synthetic sea water from 273.15 to 318.15 K. J. Chem. Thermodyn. **22** 113–27. doi:10.1016/0021-9614(90)90074-Z

Dickson, A. G., J. D. Afghan, and G. C. Anderson. 2003. Reference materials for oceanic CO_2 analysis: A method for the certification of total alkalinity. Mar. Chem. **80** 185–97. doi:10.1016/S0304-4203(02)00133-0

Dickson, A. G., C. L. Sabine, and J. R. Christian. 2007. Guide to best practices for ocean CO_2 measurements. PICES Special Publication 3, p. 191.

Dürr, H. H., G. G. Laruelle, C. M. van Kempen, C. P. Slomp, M. Meybeck, and H. Middelkoop. 2011. Worldwide typology of nearshore coastal systems: Defining the estuarine filter of river inputs to the oceans. Estuar. Coast. **34** 441–58. doi:10.1007/s12237-011-9381-y

Fagan, K. E., and F. T. Mackenzie. 2007. Air–sea CO_2 exchange in a subtropical estuarine-coral reef system, Kaneohe Bay, Oahu, Hawaii. Mar. Chem. **106** 174–91. doi:10.1016/j.marchem.2007.01.016

Gardner, W. S., M. J. McCarthy, S. An, D. Sobolev, K. S. Sell, and D. Brock. 2006. Nitrogen fixation and dissimilatory nitrate reduction to ammonium (DNRA) support nitrogen dynamics in Texas estuaries. Limnol. Oceanogr. **51** 558–68. doi:10.4319/lo.2006.51.1_part_2.0558

Gran, G. 1952. Determination of the equivalence point in potentiometric titrations. Part II. Analyst **77** 661–71. doi:10.1039/AN9527700661

Ho, D. T., N. Coffineau, B. Hickman, N. Chow, T. Koffman, and P. Schlosser. 2016. Influence of current velocity and wind speed on air–water gas exchange in a mangrove estuary. Geophys. Res. Lett. **43** 3813–21. doi:10.1002/2016GL068727

Hsu, S. A., E. A. Meindl, and D. B. Gilhousen. 1994. Determining the power-law wind-profile exponent under near-neutral stability conditions at sea. J. Appl. Meteorol. **33** 757–65. doi:10.1175/1520-0450(1994)033<0757:DTPLWP>2.0.CO;2

Hu, X., J. B. Pollack, M. R. McCutcheon, P. A. Montagna, and Z. Ouyang. 2015. Long-term alkalinity decrease and acidification of estuaries in northwestern Gulf of Mexico. Environ. Sci. Technol. **49** 3401–9. doi:10.1021/es505945p

Hunt, C. W., J. E. Salisbury, D. Vandemark, and W. McGillis. 2010. Contrasting carbon dioxide inputs and exchange in three adjacent New England estuaries. Estuar. Coast. **34** 68–77. doi:10.1007/s12237-010-9299-9

Hunt, C. W., J. E. Salisbury, and D. Vandemark. 2013. CO_2 input dynamics and air–sea exchange in a large New England estuary. Estuar. Coast. **37** 1078–91. doi:10.1007/s12237-013-9749-2

Jiang, L. Q., W. J. Cai, and Y. Wang. 2008. A comparative study of carbon dioxide degassing in river- and marine-dominated estuaries. Limnol. Oceanogr. **53** 2603–15. doi:10.4319/lo.2008.53.6.2603

Joesoef, A., W. J. Huang, Y. Gao, and W. J. Cai. 2015. Air–water fluxes and sources of carbon dioxide in the Delaware Estuary: Spatial and seasonal variability. Biogeosciences **12** 6085–101. doi:10.5194/bg-12-6085-2015

Koné, Y.-M., and A. Borges. 2008. Dissolved inorganic carbon dynamics in the waters surrounding forested mangroves of

the Ca Mau Province (Vietnam). Estuar. Coast. Shelf Sci. **77** 409–21. doi:10.1016/j.ecss.2007.10.001

Laruelle, G. G., H. H. Dürr, C. P. Slomp, and A. V. Borges. 2010. Evaluation of sinks and sources of CO_2 in the global coastal ocean using a spatially-explicit typology of estuaries and continental shelves. Geophys. Res. Lett. **37** 15. doi:10.1029/2010gl043691

Lewis, E., and D. Wallace. 1998. Program developed for CO_2 system calculations. Carbon Dioxide Information Analysis Center, Oak Ridge National Laboratory, US Department of Energy Tennessee.

Liu, Q. and others 2017. Carbonate system biogeochemistry in a subterranean estuary—Waquoit Bay, USA. Geochim. Cosmochim. Acta **203**: 422–439. doi:10.1016/j.gca.2017.01.041

Longley, W. L. 1994. Freshwater inflows to Texas bays and estuaries: Ecological relationships and methods for determination of needs. Texas Water Development Board and Texas Parks and Wildlife Department.

Millero, F. J. 2010. Carbonate constants for estuarine waters. Mar. Freshw. Res. **61** 139–42. doi:10.1071/MF09254

Millero, F. J., W. T. Hiscock, F. Huang, M. Roche, and J. Z. Zhang. 2001. Seasonal variation of the carbonate system in Florida Bay. Bull. Marine Sci. **68** 101–23.

Milliman, J. D., K. L. Farnsworth, P. D. Jones, K. H. Xu, and L. C. Smith. 2008. Climatic and anthropogenic factors affecting river discharge to the global ocean, 1951–2000. Global Planet. Change **62** 187–94. doi:10.1016/j.gloplacha.2008.03.001

Montagna, P., T. A. Palmer, and J. Pollack. 2012. Hydrological Changes and Estuarine Dynamics. Springer Science & Business Media.

Montagna, P. A., X. Hu, T. A. Palmer, and M. Wetz. 2018. Effect of hydrological variability on the biogeochemistry of estuaries across a regional climatic gradient. Limnol. Oceanogr. **63** 2465–78. doi:10.1002/lno.10953

Mooney, R. F., and J. W. McClelland. 2012. Watershed export events and ecosystem responses in the Mission–Aransas National Estuarine Research Reserve, South Texas. Estuar. Coast. **35** 1468–85. doi:10.1007/s12237-012-9537-4

Murgulet, D., V. Murgulet, N. Spalt, A. Douglas, and R. G. Hay. 2016. Impact of hydrological alterations on river-groundwater exchange and water quality in a semi-arid area: Nueces River, Texas. Sci. Total Environ. **572** 595–607. doi:10.1016/j.scitotenv.2016.07.198

Murgulet, D., M. Trevino, A. Douglas, N. Spalt, X. Hu, and V. Murgulet. 2018. Temporal and spatial fluctuations of groundwater-derived alkalinity fluxes to a semiarid coastal embayment. Sci. Total Environ. **630** 1343–59. doi:10.1016/j.scitotenv.2018.02.333

Orr, J. C., J.-M. Epitalon, A. G. Dickson, and J.-P. Gattuso. 2018. Routine uncertainty propagation for the marine carbon dioxide system. Mar. Chem. **207** 84–107. doi:10.1016/j.marchem.2018.10.006

Peterson, D. H. 1979. Sources and sinks of biologically reactive oxygen, carbon, nitrogen, and silica in northern San Francisco Bay. In San Francisco Bay—the urbanized estuary. American Association for the Advancement of Science, Pacific Division, 175–94.

Raymond, P. A., J. E. Bauer, and J. J. Cole. 2000. Atmospheric CO_2 evasion, dissolved inorganic carbon production, and net heterotrophy in the York River estuary. Limnol. Oceanogr. **45** 1707–17. doi:10.4319/lo.2000.45.8.1707

Raymond, P. A., and J. J. Cole. 2001. Gas exchange in rivers and estuaries: Choosing a gas transfer velocity. Estuar. Coast. **24** 312–7. doi:10.2307/1352954

Reyna, N. E., A. Hardison, and Z. Liu. 2017. Influence of major storm events on the quantity and composition of particulate organic matter and the phytoplankton community in a subtropical estuary. Texas Front. Marine Sci **4** 43. doi:10.3389/fmars.2017.00043.

Rosentreter, J. A., D. T. Maher, D. T. Ho, M. Call, J. G. Barr, and B. D. Eyre. 2017. Spatial and temporal variability of CO_2 and CH_4 gas transfer velocities and quantification of the CH4 microbubble flux in mangrove dominated estuaries. Limnol. Oceanogr. **62** 561–78. doi:10.1002/lno.10444

Russell, M. J., P. A. Montagna, and R. D. Kalke. 2006. The effect of freshwater inflow on net ecosystem metabolism in Lavaca Bay, Texas. Estuar. Coast. Shelf Sci. **68** 231–44. doi:10.1016/j.ecss.2006.02.005

Russell, M. J., and P. A. Montagna. 2007. Spatial and temporal variability and drivers of net ecosystem metabolism in western Gulf of Mexico estuaries. Estuar. Coast. **30** 137–53. doi:10.1007/BF02782974

Sippo, J. Z., D. T. Maher, D. R. Tait, C. Holloway, and I. R. Santos. 2016. Are mangroves drivers or buffers of coastal acidification? Insights from alkalinity and dissolved inorganic carbon export estimates across a latitudinal transect. Global Biogeochem. Cy. **30** 753–66. doi:10.1002/2015GB005324

Stets, E. G., V. J. Kelly, and C. G. Crawford. 2014. Long-term trends in alkalinity in large rivers of the conterminous US in relation to acidification, agriculture, and hydrologic modification. Sci. Total Environ. **488-489** 280–9. doi:10.1016/j.scitotenv.2014.04.054

Wanninkhof, R. 1992. Relationship between wind speed and gas exchange. J. Geophys. Res. Ocean **97** 7373–82. doi:10.1029/92JC00188

Weiss, R. F. 1974. Carbon dioxide in water and seawater: The solubility of a non-ideal gas. Mar. Chem. **2** 203–15. doi:10.1016/0304-4203(74)90015-2

Weiss, R. F., and B. A. Price. 1980. Nitrous oxide solubility in water and seawater. Mar. Chem. **8** 347–59. doi:10.1016/0304-4203(80)90024-9

Yao, H., and X. Hu. 2017. Responses of carbonate system and CO_2 flux to extended drought and intense flooding in a semiarid subtropical estuary. Limnol. Oceanogr. **62** S112–30. doi:10.1002/lno.10646

Zeng, F.-W., C. A. Masiello, and W. C. Hockaday. 2011. Controls on the origin and cycling of riverine dissolved inorganic carbon in the Brazos River, Texas. Biogeochemistry **104** 275–91. doi:10.1007/s10533-010-9501-y

Acknowledgments

We are grateful for the fieldwork assistance provided by the staff and students at both the Mission Aransas National Estuarine Research Reserve and Harte Research Institute from Texas A&M University-Corpus Christi. The fieldwork portion of this study was funded by NOAA NOS National Center for Coastal Ocean Science (Contract No. NA15NOS4780185). X.H. also acknowledges support from NSF Chemical Oceanography Program (OCE #1654232). Partial funding to this work was provided by the Texas Research Development Fund from the Research and Commercialization Office of Texas A&M University-Corpus Christi. This research was also supported in part by operations grants to the Mission-Aransas National Estuarine Research Reserve from NOAA's Office of Coastal Management. System-Wide Monitoring Program data were collected by the research staff of the Mission-Aransas NERR and hosted by the Central Data Management Office of the National Estuarine Research Reserve System.

Conflict of Interest

None declared.

Submitted 17 January 2019
Revised 21 May 2019
Accepted 16 November 2019

Associate editor: Steeve Comeau